Heliyon

ELSEVIER

Received:
22 August 2015
Revised:
2 February 2016
Accepted:
22 March 2016

Heliyon 2 (2016) e00094

Influence of microstructural features on thermal expansion coefficient in graphene/epoxy composites

Zhan Shi [a,*], Xiao-Fei Li [a], Hua Bai [a], Wei-Wei Xu [b], Shui-Yuan Yang [a], Yong Lu [a], Jia-Jia Han [a], Cui-Ping Wang [a], Xing-Jun Liu [a,*], Wei-Bin Li [b]

[a] *Department of Materials Science and Engineering, Fujian Key Laboratory of Materials Genome, College of Materials, Xiamen University, Xiamen 361005, PR China*

[b] *School of Aerospace Engineering, Xiamen University, 361005, PR China*

* Corresponding authors.

E-mail addresses: shizhan@xmu.edu.cn (Z. Shi), lxj@xmu.edu.cn (X.-J. Liu).

Abstract

In this paper, theoretical calculations were conducted to determine the coefficient of thermal expansion (CTE) based on the effective medium approach using Green's function method. The influences of microstructural features were investigated, including volume fraction, aspect ratio, and the orientation of graphene fillers. Calculated results demonstrated strong anisotropy of CTE when all graphene sheets in the composite were aligned in the in-plane direction due to the large difference between the elastic moduli of the graphene and epoxy. The in-plane CTE in the graphene/epoxy composite can be effectively reduced with small additions of graphene additive. Orientation dispersion among the graphene fillers significantly decreases the anisotropy of CTE. Accounting for the influences of all microstructural features, simulation results closely align with current experimental results. This work will provide a general guideline and a solid foundation for the optimal design and preparation of graphene/polymer composites.

Keywords: Materials science, Engineering

http://dx.doi.org/10.1016/j.heliyon.2016.e00094

1. Introduction

Composites which utilize nano-scale materials as fillers have great potential to outperform conventional composite materials which employ traditional fillers [1, 2]. Graphene, as a two-dimensional nanomaterial with a high surface area and large geometric anisotropy, has attracted tremendous attention since its discovery due to its extraordinary physical properties [3, 4, 5, 6]. Lee et al. [7] have determined the elastic modulus and theoretical strength of graphene to be as high as 1 TPa and 130 GPa, respectively. These properties identify graphene as an optimal reinforcement filler for the production of composites with a nano-sized component. As reported in previous research [8, 9, 10, 11, 12, 13], the modulus and glass transition temperature of composites can be effectively increased with the use of graphene as an additive to epoxy resin. Graphene also demonstrates high electrical and thermal conductivity, such as that of graphite and carbon nanotubes [14, 15, 16].

A low thermal expansion coefficient and good thermal stability are necessary to the use of composites in situations in which the temperature changes dramatically, such as the use of composite coatings on the surfaces of aircraft, aerospace craft, submarines and buildings. Numerous experiments which have focused on graphene/polymer composites have revealed that graphene can efficiently reduce the coefficient of thermal expansion of a polymer matrix [9, 10, 17, 18]. It has also been determined that the distribution and the orientation of graphene fillers greatly influences the performance of graphene composites [13, 17, 19]. Shiu et al. [18] have theoretically calculated the thermal and mechanical properties of graphene/epoxy composites according to molecular dynamics (MD) simulation, in which the increased Young's modulus, glass transition temperature and decreased CTE were provided. The influence of the aspect ratio and volume fraction of graphene on the CTE of a graphene/polymer composite has also been determined by the use of microscopic mechanical models [20, 21] in which graphene is considered as an ellipsoid inclusion. It has also been confirmed that the in-plane CTE of a graphene/polymer composite decreases in conjunction with an increasing graphene volume fraction and a decreasing graphene aspect ratio. However, there is no existing model developed to consider the influence of the orientation of the graphene in composites, despite the importance of graphene orientation as a microstructural feature. Hence, this paper provides a comprehensive model of CTE in graphene/polymer composites, in which the influences of numerous microstructural features can be simulated simultaneously, including the volume faction, aspect ratio, and orientation of graphene.

http://dx.doi.org/10.1016/j.heliyon.2016.e00094

2. Methods

The geometrical model of a graphene/epoxy composite is shown in Fig. 1. The graphene platelet is assumed to be ellipsoidal in shape, in which the aspect ratio ρ ($\rho = a_3/a_1$) represents the shape of graphene. All graphene platelets are embedded in the epoxy matrix, thus forming a graphene/epoxy two-phase composite with a perfect interface.

The constitutive equation for thermal expansion behavior can be expressed as follows:

$$\sigma = c(\varepsilon - \alpha\Delta T) \tag{1}$$

where σ, c, ε, α, and ΔT represent the stress, elastic modulus, strain, thermal expansion coefficient and temperature change, respectively.

In a state of static equilibrium, the stress in the composite can be expressed as follows:

$$\partial\sigma_{ij}(x)/\partial x_j = 0 \tag{2}$$

Considering the composite as a homogeneous reference medium with stiffness fluctuation, the local stiffness can be expressed as follows:

$$c = c^0 + c'(x) \tag{3}$$

where c° and c' represent the stiffness and fluctuation of the homogeneous reference medium, respectively. For convenience, the reference medium is chosen as the matrix. Eq. (2) can be solved in terms of Green's function technique [22, 23, 24, 25, 26, 27], and the local strain field within the composite can be expressed as follows:

$$\varepsilon = \varepsilon^0 + G^u(c'\varepsilon - c\alpha\Delta T) \tag{4}$$

where ε° and G^u represent the strain and the modified displacement Green's function [28] for the homogeneous medium, respectively. The iteration of

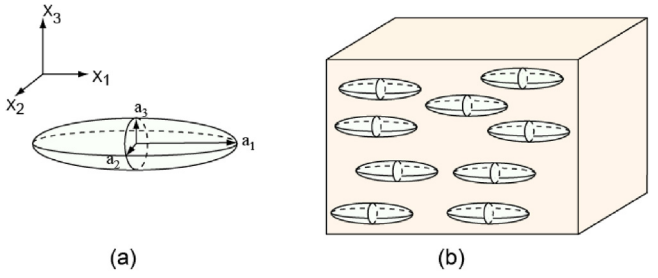

Fig. 1. Schematic diagram of graphene filler. (a) The graphene is considered a flat-ellipsoidal inclusion, with $a_1 = a_2 \neq a_3$. (b) The microstructure of a graphene/epoxy composite, assuming that all a_3 axes are parallel to x_3.

http://dx.doi.org/10.1016/j.heliyon.2016.e00094

Eq. (4) and introduction of the T matrix yields:

$$\varepsilon = T^{66}\varepsilon^0 - T^{66}G^u c\alpha\Delta T$$
$$T^{66} = (I - G^u c')^{(-1)} \tag{5}$$

where I represents the unit tensor. The effective properties of the graphene/epoxy composite can be defined in terms of the averaged method:

$$< \sigma >= c^*(< \varepsilon > -\alpha^*\Delta T) \tag{6}$$

where the angular bracket denotes the ensemble average, and c^* and α^* represent the effective stiffness and CTE of the composite, respectively. According to Eq. (5), the averaged strain is expressed as follows:

$$< \varepsilon >=< T^{66} > \varepsilon^0 - c^* < T^{66}G^u c\alpha\Delta T > -c^*\alpha^*\Delta T \tag{7}$$

By substituting Eq. (7) into Eq. (6), at the following is obtained:

$$< \sigma >= c^* < T^{66} > \varepsilon^0 - c^* < T^{66}G^u c\alpha\Delta T > -c^*\alpha^*\Delta T \tag{8}$$

Alternatively, by substituting Eq. (5) into Eq. (1) and averaging the ensemble, at the following is obtained:

$$< \sigma >=< cT^{66} > \varepsilon^0 - < cT^{66}G^u c\alpha\Delta T > - < c\alpha\Delta T > \tag{9}$$

By comparing Eq. (9) to Eq. (8) and performing simple algebraic operations, the effective properties of the composites can be expressed as follows:

$$c^* =< cT^{66} > < T^{66} >^{(-1)} \tag{10}$$

$$\alpha^* = c^{*-1} < [I - (c^* - c)T^{66}G^u]c\alpha > \tag{11}$$

Eq. (10) and Eq. (11) represent the universal solutions for the effective stiffness c^* and CTE of a graphene/epoxy composite. Eq. (11) demonstrates that the effective CTE α^* also serves as the function of CTE and the elastic coefficient of each constitutive phase, as in the law of mixtures. The term $[I\text{-}(c^*\text{-}c)T^{66}G^u]c\alpha$ inside the angular bracket in Eq. (11) represents the inner force induced by the thermal expansion of each constitutive phase. It should to be noted that the angular brackets in all equations denote the ensemble average of all microstructural features of each phase, which includes the common volume average directly related to the volume fractions, and the orientation average of all possible graphene orientations in the composite. While determining the orientation average, the terms inside the angular bracket will be converted into the values of the macroscopic coordinate system, and then averaged according to the distribution probability of the filler's orientation [27]. For example, the orientation average of a four-rank tensor X_{ijkl} for the transversely isotropic composite is expressed as follows:

http://dx.doi.org/10.1016/j.heliyon.2016.e00094

$$< X_{ijkl} >_{orientation} = \int \beta_{im}\beta_{jn}\beta_{kp}\beta_{lq}X'_{mnpq}F(\theta)\sin(\theta)d\theta / \int F(\theta)\sin(\theta)d\theta \quad (12)$$

where $F(\theta)$ is a distribution function describing the variation in the Euler angle θ of the local x'_3 axis with respect to the sample x_3 axis, β is the coordinate transformation matrix, and X'_{mnpq} are the corresponding quantities in the individual particles.

The code used for simulation was developed by the LabVIEW language, which is a graphical programming platform and a convenient development environment. The code involves five main modules, which are materials' properties input module, Green's function module, T matrix module, average module, and effective properties module. During the calculation, firstly, the properties of filler and matrix were input, such as Young's modulus, Poisson's ratio, and thermal expansion coefficient. Secondly, the Green's function G^u was gained by Green's function module, using C° and aspect ratio. Thirdly, the T matrix in matrix and filler was calculated. They can be denoted as T_m and T_f. Fourthly, the ensemble average was calculated in average module, including the orientation average and the common volume average. That is $<F> = V_m<F_m>_{orientation} + V_f<F_f>_{orientation}$, where F is the function to be averaged. Finally, by simple matrix calculation in Eq. (10) and Eq. (11), the effective properties of composites were obtained.

Without considering the effect of orientation dispersions, the proposed model will in accordance with Mori-Tanaka's method [29]. In previous models determined by the microscopic mechanical method [20, 21], the effect of the orientation dispersion of the fillers has not been considered. Compared to previous models, the superiority of the proposed model is achieved by the consideration of the effect of orientation dispersion.

3. Results and discussion

A comparison was conducted between the proposed model and previous models to verify the validity of the proposed model. In this situation, all fillers are assumed to be in perfect alignment in the composite. As shown in Fig. 2, the calculated CTE of glass fiber/epoxy composites according to the proposed model was compared to previous calculated results determined by other models [21, 30, 31]. The aspect ratio ρ was set to 100, *i.e.* $a_3/a_1 = 100$. The necessary parameters used in the calculation were obtained from previous literature as listed in Table 1.

As demonstrated by Fig. 2, the results calculated by the proposed model are quite similar to those produced by other models [21, 30, 31]. Results indicated that all α^*_{11}/α_m values slightly increase with increasing f, reach a maximum, and then finally decrease as f increases, while all α^*_{33}/α_m values decrease

http://dx.doi.org/10.1016/j.heliyon.2016.e00094

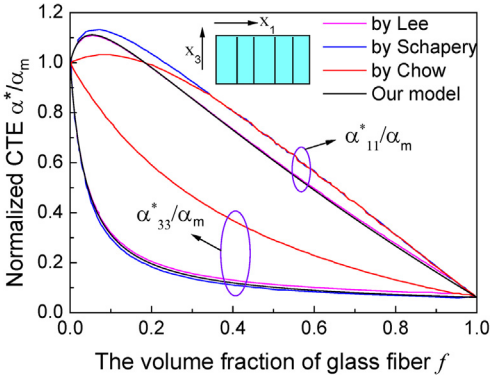

Fig. 2. Comparison of CTE in glass fiber/epoxy calculated by various models. The fixed aspect ratio $\rho = 100$ for Chow's, Lee's and the proposed model, and $\rho = \infty$ for Schapery's model. The inset is the schematic diagram of the microstructure of glass fiber/epoxy, in which the fibers are perfect alignment.

continuously with increasing *f*. All α^*_{33}/α_m results from the proposed model are in agreement with results obtained with Lee's [21] and Schapery's [30] models.

In addition, α^*_{11}/α_m, results from as calculated by the proposed model are nearly identical to those calculated by Schapery's model. Calculations from all four analyzed models demonstrate a slight increase in α^*_{11}/α_m when the volume fraction of glass fiber is less than 0.1, indicating that a small addition of glass fiber results in an increase of the composite CTE in the transverse direction. According to the rule of mixtures, if glass fiber demonstrates a lower CTE than that of the epoxy, the CTE of the overall composite will be lower than that of the epoxy. The "abnormal" increase of the CTE in composites is derived from the strong microstructural anisotropy of the composite. If the length of the glass fiber is greater than the diameter, the thermal expansion in the longitudinal direction of the epoxy is strongly constrained by the glass fiber; this strong constraint in the longitudinal direction will result in a disguised expansion in the transversal direction according to the constant-volume principle. When the

Table 1. Properties of graphene, glass fiber, PEId, graphene nanoplatelets (GNP) and epoxy.

	Young's modulus (GPa)	Linear CTE ($\times 10^{-6}$/ °C)	Poisson's ratio
Epoxy [21]	2.76	81	0.35
PEId [20]	3.13	55.83	0.36
Glass fiber [21]	72.4	5.0	0.20
GNP [20]	1060	7.83	0.006
Graphene	1050 [32]	20 [33]	0.186 [32]

http://dx.doi.org/10.1016/j.heliyon.2016.e00094

volume fraction of the glass fiber is small, this anisotropic disguised expansion effect may overcome the reduced effect from the glass fiber, resulting in an α^*_{11}/α_m value greater than 1.

After verifying the validity of the proposed model, a detailed study was conducted to investigate graphene/polymer composites. Fig. 3 demonstrates the effective CTE as a function of the volume fraction of the graphene filler for a fixed aspect ratio $\rho = 0.01$. Fig. 3 depicts the effective CTE as a function of the volume fraction of the graphene filler, with the glass fiber/epoxy results of $\rho = 100$ plotted as a reference. Results indicate that the CTE decreases more dramatically in graphene/epoxy composites than in glass fiber/epoxy composites. The α^*_{11}/α_m can be reduced by approximately 50% by adding only a 5% volume fraction of graphene, while a nearly 10% volume fraction of glass fiber must be added to achieve a 50% reduction of α^*_{11}/α_m. For different matrices, the graphene/epoxy composite demonstrates a greater rate of decrease CTE than that of graphene/PEId, which might be due to the lower Young's modulus of epoxy. As shown in Fig. 3(b) the practical CTE of graphene/PEId possesses a lower CTE due to the lower CTE value of PEId as compared to epoxy.

The CTE of graphene/epoxy composites was then calculated as a function of the aspect ratio ρ for four fixed volume fractions of graphene: 0.05, 0.1, 0.15, and

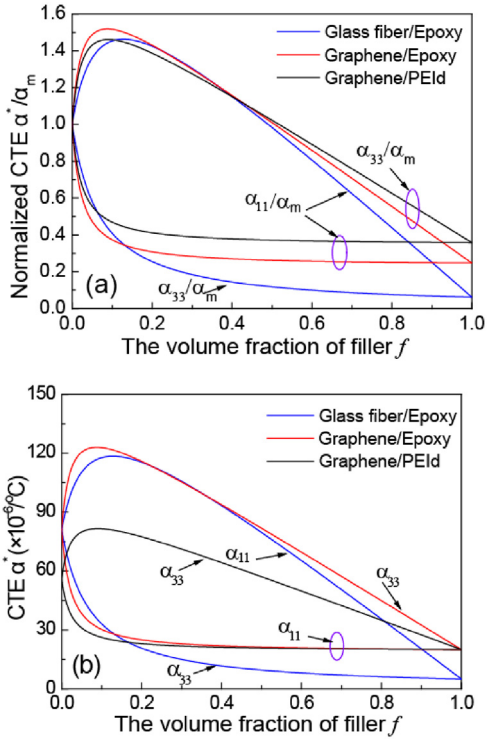

Fig. 3. The relationship between calculated CTE and volume fraction of the graphene or glass fiber for fixed aspect ratio $\rho = 0.01$.

http://dx.doi.org/10.1016/j.heliyon.2016.e00094

0.2. As shown in Fig. 4, results indicated that for each fixed volume fraction *f*, when the inclusion has a spherical shape ($\rho = 1$), the composites will become isotropic, i.e. $\alpha^*_{33} = \alpha^*_{11}$. The anisotropy of CTE increases as the aspect ratio decreases. As shown in Fig. 4, results indicate that with the ideal microstructure of Fig. 1(b), α^*_{11} will significantly decrease as the aspect ratio of graphene decreases. Therefore, if the graphene/polymer composite is used as a coating, it is necessary to ensure a large in-plane graphene sheet, which will strongly reduce the in-plane CTE and avoid disbanding when the surface temperature undergoes dramatic change.

In the calculations above, the distribution of the graphene filler is assumed to be perfectly oriented along the x_3 direction (Fig. 1(b)). However, graphene fillers in the composites might randomly distribution as shown in Fig. 5(a). Therefore, the influence of the orientation of the graphene filler was simulated by the proposed model. As shown in Fig. 5(b), if the projection of the a_3 axis of each graphene filler is regarded as a projection sphere with an infinite radius, the orientations of graphene fillers can be represented by the probability of the distribution of the projection points on the surface of the projection sphere. Assuming that the projection points are distributed uniformly within a cone with a half-cone-angle of $\theta_{\text{cut-off}}$, the distribution of the graphene fillers can be qualitatively represented by $\theta_{\text{cut-off}}$. For example, if $\theta_{\text{cut-off}} = 0°$, all the a_3 axes of graphene fillers align along the x_3 direction, representing the ideal microstructure as presented in Fig. 1(b). If $\theta_{\text{cut-off}} = 90°$, the projection cone becomes a semi-sphere, representing a random distribution. After the introduction of $\theta_{\text{cut-off}}$, the orientation average of the graphene distribution is accounted for by Eq. (11). $\theta_{\text{cut-off}}$ is the upper limit in the integration in Eq. (12). The relationship between the CTE of the graphene/epoxy composite and the distribution cut-off angle $\theta_{\text{cut-off}}$ was calculated for three fixed aspect ratios: 0.1, 0.01, and 0.001. The calculated results are illustrated in Fig. 6.

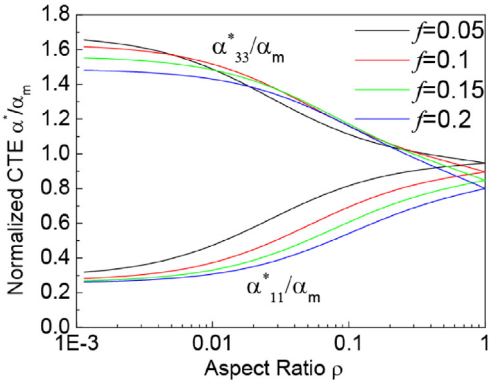

Fig. 4. Normalized CTE of graphene/epoxy composite as a function of aspect ratio ρ for various graphene volume fractions *f*.

http://dx.doi.org/10.1016/j.heliyon.2016.e00094

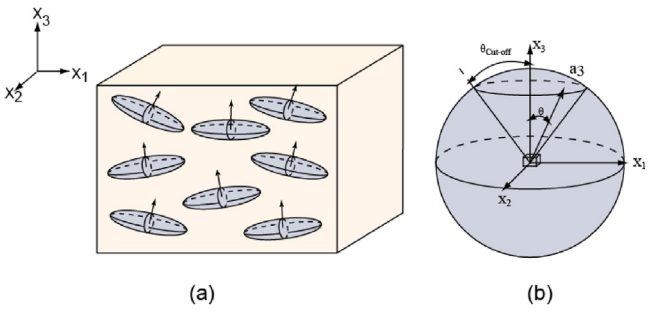

Fig. 5. (a) Schematic diagram of the distribution of graphene fillers in graphene/epoxy composite. (b) The a_3 axes of graphene fillers in the composite are assumed to be uniformly distributed within a distribution projection cone with a half-cone angle $\theta_{\text{cut-off}}$.

Fig. 6 shows the CTE of graphene/epoxy as a function of the orientation distribution cutoff angle $\theta_{\text{cut-off}}$ with different aspect ratios for fixed volume fraction $f = 0.01$ and $f = 0.1$. Generally, α^*_{33} decreases and α^*_{11} increases with increasing θ_{cutoff}. Lower aspect ratios result in more rapid changes in α^*_{33} and α^*_{11}. According to Eq. (11), the effective CTE α^* is the product of the effective compliance coefficient and the inner force term. With increasing θ_{cutoff}, the effective compliance coefficient along axis x_3 decreases and the inner force

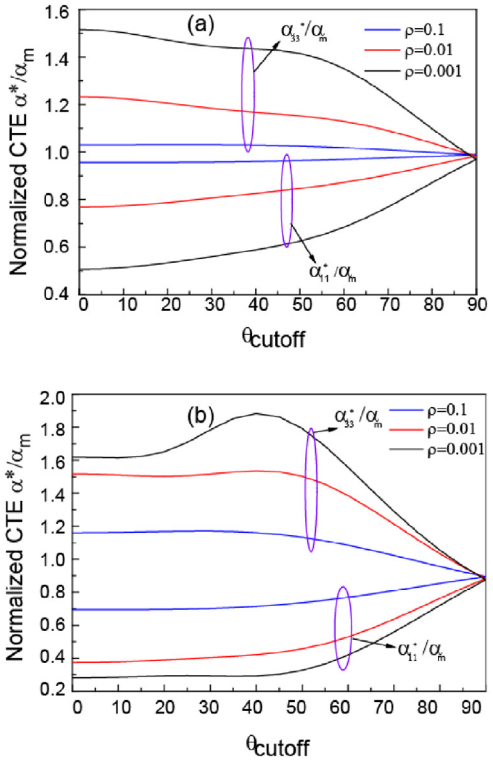

Fig. 6. Influence of the distribution cutoff angle $\theta_{\text{cut-off}}$ on the CTE with different aspect ratios in graphene/epoxy composites. (a) Volume fraction is 0.01 (b) Volume fraction is 0.1.

http://dx.doi.org/10.1016/j.heliyon.2016.e00094

increases. Generally, the effective compliance decreases more rapidly than the increase in the inner force, resulting in the decrease of the CTE α^*_{33}. For $f = 0.1$ and $\rho = 0.001$, in the range of $\theta_{cutoff} = 20–55°$, α^*_{33} demonstrates an obvious increase with increasing θ_{cutoff}; this increase of α^*_{33} implies that the inner force increases more rapidly. This phenomenon does not appear very clearly when the aspect ratio is 0.01 or 0.1. Therefore it can be concluded that a lower aspect ratio results in higher anisotropy and greater inner force. When $\theta_{cutoff} = 90°$, α^*_{33} and α^*_{11} are identical, indicating that α^* becomes isotropic; this is in agreement with the random distribution of graphene fillers when $\theta_{cutoff} = 90°$. The relationship between the effective CTE and the volume fraction of graphene was calculated for three fixed orientation distribution cutoff angles, as shown in Fig. 7.

Finally, a comparison between calculated results and experimental data was conducted. Fig. 8 displays the simulation results of the proposed model and the experimental results of GNP/PEId and graphene/epoxy composites. The parameters used in the simulation are listed in Table 1. According to the experimental results, the aspect ratio of the simulation was set to 0.02 for GNP/PEId [20] and 0.001 for graphene/epoxy [12]. The orientation angle distribution can be measured by SEM following further image analysis [20]. According to

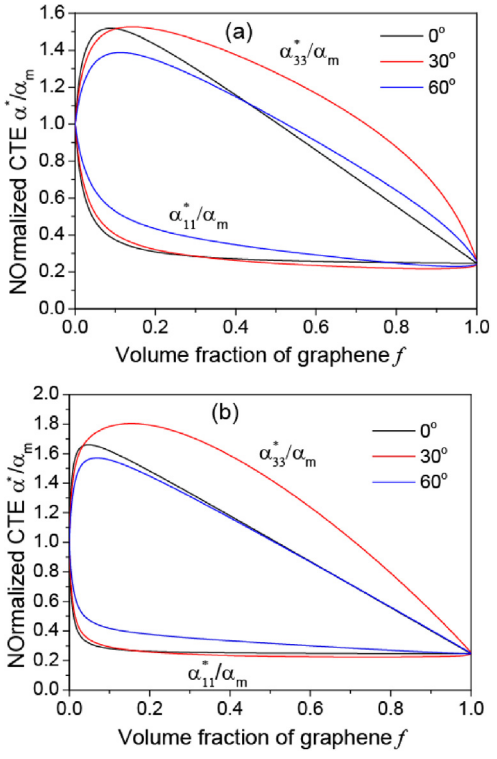

Fig. 7. Dependence of the thermal expansion coefficient on volume fraction f in graphene/epoxy composites for $\theta_{cutoff} = 0°$, 30° and 60° with (a) $\rho = 0.01$ and (b) $\rho = 0.001$.

http://dx.doi.org/10.1016/j.heliyon.2016.e00094

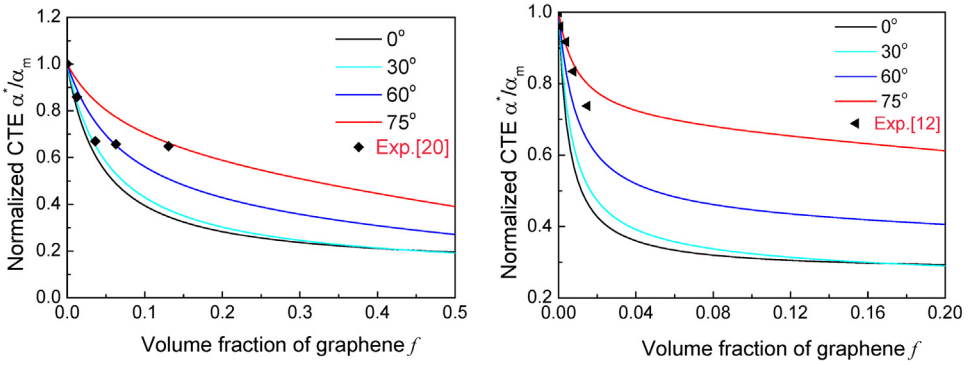

Fig. 8. Comparison of calculated results with various θ_{cutoff} and experimental data. (a) GNP/PEId, $\rho = 0.02$ [20]. (b) Graphene/epoxy, $\rho = 0.001$ [12].

the measured orientation distribution data, a very obvious dispersion of the orientation angle was confirmed in real composites. Hence, three orientation distribution cut-off angles $\theta_{cut\text{-}off}$ were assumed as 30°, 60°, and 75°. As shown in Fig. 8(a), the simulated results closely align with experimental results; therefore, it is possible to conclude that the orientation of graphene fillers strongly influences the thermal expansion coefficient. Additionally, as shown in Fig. 8(b), with an aspect ratio of 0.001, the experimental results are also in agreement with the simulated results of $\theta_{cutoff} = 60°–75°$ [12].

4. Conclusions

A theoretical model using Green's function method and the effective medium approach was designed to simulate the thermal expansion behavior of graphene/epoxy composites. After verification, results achieved by the proposed model were in good agreement with results produced by previous models. Additionally, the proposed model effectively simulated the influence of the orientation distribution of graphene fillers in graphene/epoxy composites. Results demonstrated that microstructural features greatly influence the thermal expansion behavior of graphene/epoxy composites. Strong CTE anisotropy was observed in all simulated results due to the large geometric anisotropy of graphene and the large difference between the elastic coefficients of graphene and the polymer matrix. For an ideal microstructure in which all graphene aligns perfectly, a significant decrease of the in-plane thermal expansion coefficient can be achieved with a very small amount of graphene additive. The dispersion of the orientation of graphene will also decrease the anisotropy of the CTE. After the introduction of the distribution cutoff angle in the proposed model, calculation results were in good agreement with experimental results. This work is expected to provide a general guideline for the further development of graphene/polymer composites.

http://dx.doi.org/10.1016/j.heliyon.2016.e00094

Declarations

Author contribution statement

Zhan Shi, Xiao-Fei Li: Conceived and designed the experiments; Performed the experiments; Wrote the paper.

Hua Bai, Wei-Wei Xu, Shui-Yuan Yang, Yong Lu, Jia-Jia Han, Cui-Ping Wang, Xing-Jun Liu, Wei-Bin Li: Analyzed and interpreted the data.

Funding statement

This work was supported by The Fundamental Research Funds for the Central Universities (No. 20720140511) and the National Natural Science Foundation of China (No. 51201145, and No. 1301146).

Competing interest statement

The authors declare no conflict of interest.

Additional information

No additional information is available for this paper.

References

[1] T. Ramanathan, A.A. Abdala, S. Stankovich, D.A. Dikin, M. Herrera-Alonso, R.D. Piner, et al., Functionalized graphene sheets for polymer nanocomposites, Nat. Nanotechnol. 3 (6) (2008) 327–331.

[2] M.A. Rafiee, J. Rafiee, Z. Wang, H. Song, Z.-Z. Yu, N. Koratkar, Enhanced Mechanical Properties of Nanocomposites at Low Graphene Content, ACS Nano 3 (12) (2009) 3884–3890.

[3] D.A. Dikin, S. Stankovich, E.J. Zimney, R.D. Piner, G.H. Dommett, G. Evmenenko, et al., Preparation and characterization of graphene oxide paper, Nature 448 (7152) (2007) 457–460.

[4] K.S. Novoselov, A.K. Geim, S. Morozov, D. Jiang, Y. Zhang, S. Dubonos, et al., Electric field effect in atomically thin carbon films, Science 306 (5696) (2004) 666–669.

[5] S. Stankovich, D.A. Dikin, G.H. Dommett, K.M. Kohlhaas, E.J. Zimney, E.A. Stach, et al., Graphene-based composite materials, Nature 442 (7100) (2006) 282–286.

[6] C. Gómez-Navarro, M. Burghard, K. Kern, Elastic properties of chemically derived single graphene sheets, Nano Letters 8 (7) (2008) 2045–2049.

 http://dx.doi.org/10.1016/j.heliyon.2016.e00094

[7] C. Lee, X. Wei, J.W. Kysar, J. Hone, Measurement of the elastic properties and intrinsic strength of monolayer graphene, Science 321 (5887) (2008) 385–388.

[8] X.-J. Shen, Y. Liu, H.-M. Xiao, Q.-P. Feng, Z.-Z. Yu, S.-Y. Fu, The reinforcing effect of graphene nanosheets on the cryogenic mechanical properties of epoxy resins, Compos. Sci. Technol. 72 (13) (2012) 1581–1587.

[9] J.K. Lee, S. Song, B. Kim, Functionalized graphene sheets-epoxy based nanocomposite for cryotank composite application, Polym. Composite. 33 (8) (2012) 1263–1273.

[10] S. Wang, M. Tambraparni, J. Qiu, J. Tipton, D. Dean, Thermal expansion of graphene composites, Macromolecules 42 (14) (2009) 5251–5255.

[11] M. Martín-Gallego, R. Verdejo, M. Lopez-Manchado, M. Sangermano, Epoxy-graphene UV-cured nanocomposites, Polymer 52 (21) (2011) 4664–4669.

[12] M. Martin-Gallego, M. Hernandez, V. Lorenzo, R. Verdejo, M. Lopez-Manchado, M. Sangermano, Cationic photocured epoxy nanocomposites filled with different carbon fillers, Polymer 53 (9) (2012) 1831–1838.

[13] L.-C. Tang, Y.-J. Wan, D. Yan, Y.-B. Pei, L. Zhao, Y.-B. Li, et al., The effect of graphene dispersion on the mechanical properties of graphene/epoxy composites, Carbon 60 (2013) 16–27.

[14] R. Grantab, V.B. Shenoy, R.S. Ruoff, Anomalous strength characteristics of tilt grain boundaries in graphene, Science 330 (6006) (2010) 946–948.

[15] A.A. Balandin, S. Ghosh, W. Bao, I. Calizo, D. Teweldebrhan, F. Miao, et al., Superior thermal conductivity of single-layer graphene, Nano Letters 8 (3) (2008) 902–907.

[16] R. Nair, P. Blake, A. Grigorenko, K. Novoselov, T. Booth, T. Stauber, et al., Fine structure constant defines visual transparency of graphene, Science 320 (5881) (2008) 1308.

[17] H. Wu, L.T. Drzal, Graphene nanoplatelet-polyetherimide composites: Revealed morphology and relation to properties, J. Appl. Polym. Sci. 130 (6) (2013) 4081–4089.

[18] S.-C. Shiu, J.-L. Tsai, Characterizing thermal and mechanical properties of graphene/epoxy nanocomposites, Compos. Part B-Eng. 56 (2014) 691–697.

[19] H. Kim, C.W. Macosko, Processing-property relationships of polycarbonate/graphene composites, Polymer 50 (15) (2009) 3797–3809.

 http://dx.doi.org/10.1016/j.heliyon.2016.e00094

[20] H. Wu, L.T. Drzal, Effect of graphene nanoplatelets on coefficient of thermal expansion of polyetherimide composite, Mater. Chem. Phys. 146 (1) (2014) 26–36.

[21] K. Lee, K. Kim, S. Jeoung, S. Ju, J. Shim, N. Kim, et al., Thermal expansion behavior of composites based on axisymmetric ellipsoidal particles, Polymer 48 (14) (2007) 4174–4183.

[22] C.-W. Nan, M. Li, J.H. Huang, Calculations of giant magnetoelectric effects in ferroic composites of rare-earth–iron alloys and ferroelectric polymers, Phys. Rev. B 63 (14) (2001) 144415.

[23] C.-W. Nan, M. Li, X. Feng, S. Yu, Possible giant magnetoelectric effect of ferromagnetic rare-earth-iron-alloys-filled ferroelectric polymers, Appl. Phys. Lett. 78 (17) (2001) 2527–2529.

[24] C.-W. Nan, Effective magnetostriction of magnetostrictive composites, Appl. Phys. Lett. 72 (22) (1998) 2897–2899.

[25] C.-W. Nan, G.J. Weng, Influence of microstructural features on the effective magnetostriction of composite materials, Phys. Rev. B 60 (9) (1999) 6723.

[26] C.-W. Nan, Physics of inhomogeneous inorganic materials, Prog. Mater. Sci. 37 (1) (1993) 1–116.

[27] Z. Shi, C.-W. Nan, J. Liu, D. Filippov, M. Bichurin, Influence of mechanical boundary conditions and microstructural features on magnetoelectric behavior in a three-phase multiferroic particulate composite, Phys. Rev. B 70 (13) (2004) 134417.

[28] C.-W. Nan, L. Liu, D. Gou, L. Li, Calculations of the effective properties of 1-3 type piezoelectric composites with various rod/fibre orientations, J. Phys. D: Appl. Phys. 33 (2000) 2977–2984.

[29] C.-W. Nan, K.-F. Cai, R.-Z. Yuan, A Relation Between Multiple-Scattering Theory and Micromechanical Models of Effective Thermoelastic Properties, Ceram. Int. 22 (1996) 457–461.

[30] R.A. Schapery, Thermal expansion coefficients of composite materials based on energy principles, J. Compos. Mater. 2 (3) (1968) 380–404.

[31] T. Chow, Effect of particle shape at finite concentration on thermal expansion of filled polymers, J. Polym. Sci. Polym. Phys. Ed. 16 (6) (1978) 967–970.

 http://dx.doi.org/10.1016/j.heliyon.2016.e00094

[32] F. Liu, P. Ming, J. Li, Ab initio calculation of ideal strength and phonon instability of graphene under tension, Phys. Rev. B 76 (6) (2007) 064120.

[33] J.-W. Jiang, J.-S. Wang, B. Li, Thermal expansion in single-walled carbon nanotubes and graphene: Nonequilibrium Green's function approach, Phys. Rev. B 80 (20) (2009) 205429.

 http://dx.doi.org/10.1016/j.heliyon.2016.e00094